

A Simple Strategy to Realize Super Stable Ferroelectric Capacitor via Interface Engineering

Hyo-Bae Kim, Kyun Seong Dae, Youkyoung Oh, Seung-Won Lee, Yoseop Lee, Seung-Eon Ahn, Jae Hyuck Jang,* and Ji-Hoon Ahn*

Fluorite-structure ferroelectric thin films have been extensively studied as promising candidates for next-generation non-volatile memory. However, these ferroelectric thin films have fatal issues such as the irregular formation of the ferroelectric phase, low cycling endurance, and wake-up and fatigue during endurance cycling tests. These problems are reportedly caused by oxygen vacancies, which form due to the interface reaction between the thin films and bottom electrodes during deposition and the post-annealing process. Therefore, in this work, the enhanced ferroelectric characteristics of $\text{Hf}_{1-x}\text{Zr}_x\text{O}_2$ thin films that control the oxygen vacancies in thin films through interfacial pretreatment are investigated. Interfacial treatment using an oxygen source can reduce oxygen vacancies and improve crystallinity through intentional oxidation of the bottom electrode. As a result, the remanent polarization value is increased by ≈ 1.6 times by applying the optimized pretreatment condition, and the measured $2P_r$ is a very high value of $73 \mu\text{C cm}^{-2}$. Furthermore, it exhibits very stable ferroelectric properties without a wake-up effect or significant fatigue, up to 10^8 cycles even under a severe electric field of 3.5 MV cm^{-1} . This simple strategy provides a new avenue to effectively improve the performance and cycling endurance of devices with ferroelectric thin films.

complementary metal–oxide–semiconductor processes, which are very advantageous in terms of device design and fabrication.^[2] For this reason, the use of HfO_2 -based ferroelectric thin films in the field of nonvolatile ferroelectric memories such as ferroelectric-field effect transistors, ferroelectric-random access memory, neuromorphic devices,^[3–7] energy storage capacitors^[8] and piezoelectric devices^[9] are receiving great interest. Specifically, high-performance, nonvolatile ferroelectric memory, and neuromorphic applications require high remanent polarization (P_r) characteristics to achieve a large memory window and a uniform level of ferroelectric properties over multiple operating cycles for the high-reliability characteristics of the memory device. In addition, it is also important to withstand as many switching cycles as possible from an endurance point of view before the device endures a hard breakdown. However, the ferroelectric remanent polarization of HfO_2 -based thin films generally

increase and decrease as the measuring cycle increases due to the wake-up effect and fatigue,^[2–3,10] which is related to several reasons such as field-cycling-induced phase transition,^[11] doping concentration,^[12] and the amount of oxygen vacancies and bulk defects present in HfO_2 -based ferroelectric thin films.^[10,13–15] It is known that oxygen vacancies, which affect the endurance properties of HfO_2 -based ferroelectrics, can occur in the unwanted interface reactions and by oxygen scavenging at the electrode during deposition of ferroelectric thin films or post-annealing processes used for crystallization of the ferroelectric phase.^[2,16] These oxygen vacancies can be redistributed during the switching cycle, resulting in an increasing P_r value, called the wake-up effect. Even after wake-up, oxygen vacancies are newly generated during the electrical switching cycle. This causes domain pinning and electron trapping, which degrade ferroelectric properties during the cycle process, called fatigue, even causing hard breakdown.^[10,12,17] These unstable cyclic ferroelectric characteristics can change the operation parameters, such as the read/write voltage of the ferroelectric devices. Therefore, it is an obstacle to stable and long-term use of the device. Meanwhile, it has also been reported that an appropriate amount of oxygen vacancies in the HfO_2 -based thin film helps stabilize the orthorhombic phase, providing the structural origins of ferroelectricity.^[18–19] Pal et al. reported that the P_r value


1. Introduction

Since ferroelectricity was discovered and reported for the first time in HfO_2 -based thin films in 2011,^[1] various studies have focused on this material because of its superior ferroelectricity in relative thin films and compatibility with advanced

H.-B. Kim, Y. Oh, S.-W. Lee, J.-H. Ahn
Department of Materials Science and Chemical Engineering
Hanyang University
55 Hanyangdaehak-ro, Sangnok-gu, Ansan, Gyeonggi-do 15588, Republic of Korea
E-mail: ajh1820@hanyang.ac.kr

K. S. Dae, J. H. Jang
Electron Microscopy & Spectroscopy Team
Korea Basic Science Institute (KBSI)
Daejeon 34133, Republic of Korea
E-mail: jhjang@kbsi.re.kr

Y. Lee, S.-E. Ahn
Department of Nano & Semiconductor Engineering
Korea Polytechnic University
Siheung 15073, Republic of Korea

 The ORCID identification number(s) for the author(s) of this article can be found under <https://doi.org/10.1002/admi.202102528>.

DOI: 10.1002/admi.202102528

increased with decreasing oxygen injection time, but they did not report endurance characteristics.^[18] Additionally, Mittmann et al. reported that the concentration of oxygen determines the nucleating phase of nano-crystallites in the as-deposited films, and as the amount of injected oxygen during HfO₂ deposition by sputtering decreased, the intensity of orthorhombic phase peak increased after post crystallization annealing.^[19] An adequate amount of oxygen vacancies in HfO₂-based ferroelectric thin films can help crystallize an orthorhombic phase, but it may cause deterioration in the endurance characteristics. To improve the endurance properties, some researchers focused on the surface of the TiN bottom electrode and the interface formed with the ferroelectric thin film deposited thereon. Li et al. reported the effect of nitrogen content in TiN bottom electrodes on the ferroelectric cycling character of Hf_{1-x}Zr_xO₂ (HZO) ferroelectric capacitors. They claimed a TiN bottom electrode with higher nitrogen contents effectively suppressed the wake-up effect by reducing the concentration of oxygen vacancies in HZO thin films.^[20] Chen et al. reported that the NH₃ plasma treatment suppressed the wake-up effect of ferroelectric HZO thin films. The amount of oxygen vacancies in the HZO film effectively decreased by a NH₃ plasma treatment at the interface. As a result, they demonstrated an HZO ferroelectric capacitor free from wake-up and fatigue effects up to 10⁶ cycles.^[14] As described above, controlling the amount of oxygen in the ferroelectric thin film lost through the interfacial reaction with TiN (which is generally used as an electrode for a HfO₂ based ferroelectric capacitor) is very important for producing stable and excellent ferroelectric-based devices.

In this study, we propose a simple strategy to improve the ferroelectric performance of TiN/HZO/TiN capacitors via interface engineering of intentional interfacial oxidation. The main idea is that if interfacial oxidation of TiN cannot be avoided, the surface of TiN is intentionally oxidized using oxygen in the HZO thin film to preserve oxygen in HZO, thereby minimizing

oxygen vacancies. The HZO thin films were deposited on TiN bottom electrodes by atomic layer deposition (ALD) using ozone. Before the deposition of the HZO thin film, ozone was used as an oxidizing agent in the ALD process, flowing to oxidize TiN, and the variation of ferroelectric properties according to ozone pre-treatment was investigated. In addition, the change in crystallinity and the change in interfacial characteristics were systematically investigated to identify the reasons for changes in ferroelectric properties. Through this simple approach, we demonstrated an HZO based ferroelectric capacitor with a very high 2P_r value of 73.0 μC cm⁻² and excellent endurance results without wake-up and fatigue effects up to 10⁸ cycles even under a severe electric-field of 3.5 MV cm⁻¹.

2. Results and Discussion

The schematic of the process flow of fabricating metal–ferroelectric–metal (MFM) capacitors are shown in **Figure 1a**. First, we investigated the effect of the ozone pre-treatment on the electrical properties of TiN/HZO/TiN capacitors. **Figure 1b** shows the P-E curves of MFM capacitors swept at 3.5 MV cm⁻¹ as a function of the ozone pre-treatment time. In the case of the MFM capacitor without pre-treatment (black line), a 2P_r value of 46.4 μC cm⁻² was obtained. Within the range performed in this study, clear ferroelectric P-E characteristics were observed in all MFM capacitors regardless of the pre-treatment time, and it was also observed that the degree of polarization changed with the ozone pre-treatment time. As shown in **Figure 1c**, the 2P_r value increased and decreased based on an ozone pre-treatment time of 10 s, and the MFM capacitor with 10 s ozone pre-treatment exhibited the maximum 2P_r value of 73.0 μC cm⁻², which is ≈1.57 times (+26.6 μC cm⁻²) higher than that without pre-treatment. This increase in remanent polarization according to the ozone pre-treatment may be due to the

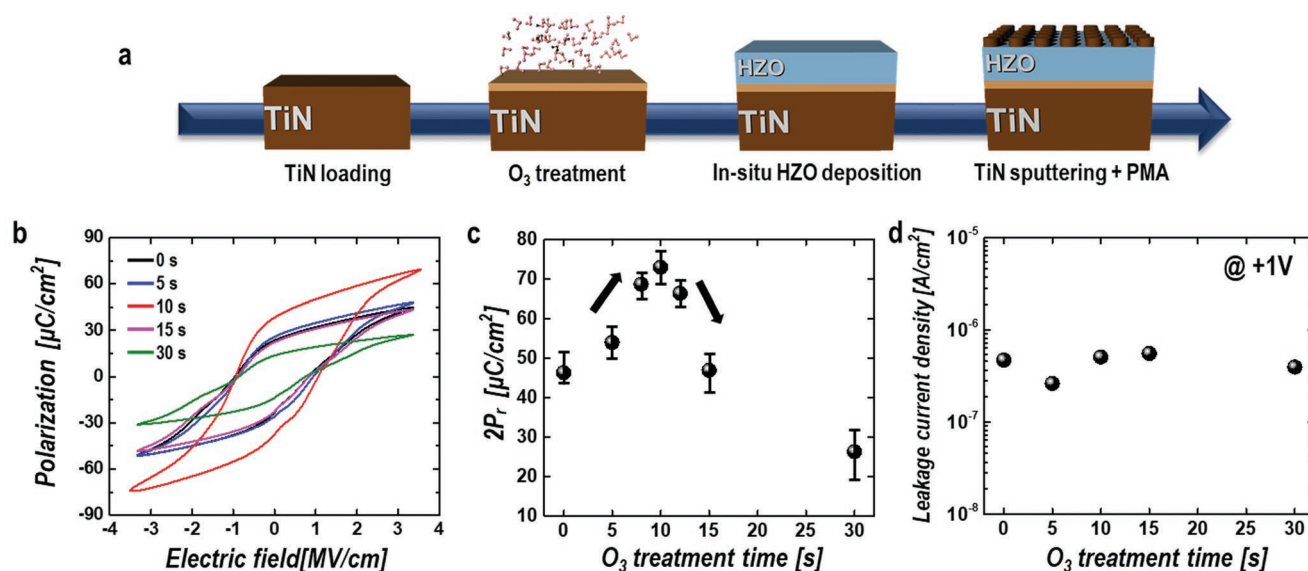


Figure 1. a) Schematic of process flow for fabricating MFM capacitors including surface treatment using ozone. b) Polarization–electric field (P–E) curves and c) variation of 2P_r values with various ozone pretreatment times. d) Variation of leakage current density measured at 1 V of MFM capacitors according to the ozone pretreatment film.

improvement of the crystallinity of the HZO thin film in the orthorhombic phase or the change in the interfacial properties between the HZO thin film and the TiN bottom electrode. It is obvious that the TiN surface is slightly oxidized through ozone treatment before HZO deposition. Meanwhile, it was observed that excessive ozone pre-treatment causes deterioration of the ferroelectric properties. In the previous study, Mittmann et al. reported that the oxygen concentration in ferroelectric HfO₂ films during the deposition process can impact the nucleation and grain growth behavior, and insufficient oxygen can produce a ferroelectric orthorhombic phase, while sufficient oxygen is more likely to produce the monoclinic phase after annealing.^[19] Accordingly, it is possible that the excessive ozone pre-treatment time, which prevents oxygen scavenging due to the TiO₂ layer formed thickly at the HZO/TiN interface, can cause a decrease in the ferroelectric orthorhombic phase. Another possibility is that the ferroelectricity of the HZO thin film is hampered by the interfacial layer of TiO₂ with paraelectric properties, which becomes thicker as the pre-treatment time increases. We confirmed that the change in ferroelectricity caused by interfacial oxidation by ozone pre-treatment is also observed in oxidation using O₂ plasma (see Figure S6, Supporting information). Interestingly, even when O₂ plasma was used as the interfacial oxidation source, almost the same ferroelectric trend was observed as when ozone was used. Therefore, it is clear that

the ferroelectric properties of MFM capacitors can be improved due to the intentional interfacial oxidation of TiN substrates induced using various oxidation sources. Meanwhile, as shown in Figure 1d and Figure S6 (Supporting information), all MFM capacitors exhibited good leakage current density properties in the range of 500 nA cm⁻² level, and there was no noticeable change in leakage current density characteristics according to ozone treatment and O₂ plasma treatment.

Next, the chemical bonding states at the interface were analyzed to investigate the cause of the improvement of ferroelectric properties by ozone pre-treatment. Figure 2a shows the normalized XPS spectra of Ti 2p core level for the interface region of 4 nm-thick HZO thin films and TiN substrates without and with ozone pre-treatment for 10 s. In the case of the HZO films deposited without pre-treatment, several chemical binding states existed, including TiN, TiN_xO_y sub-oxides, and TiO₂.^[21] This result indicates that the TiN substrate was oxidized during the HZO deposition and post-annealing process in the form of TiO₂ and TiN_xO_y. The oxygen source of this unwanted interface oxidation can be oxygen contained in the HZO thin film, so it may affect the physical properties and electrical properties of the HZO thin films. On the other hand, in the case of the ozone pre-treated sample, the intensity of the TiO₂ peak increased significantly compared to the TiN and TiN_xO_y sub-oxides peaks. The relatively sharp increase

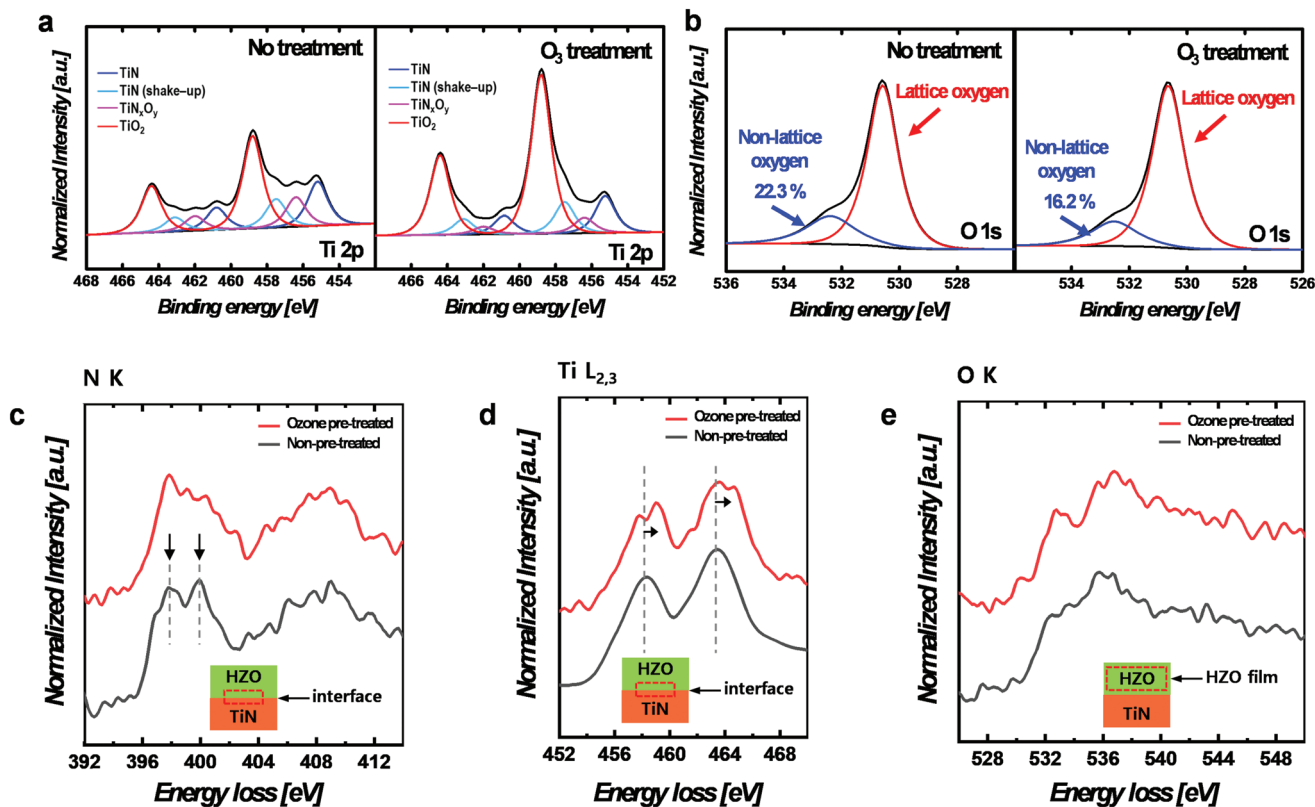


Figure 2. XPS spectra of Ti 2p core level for interface region of HZO thin films and TiN substrates: a) without pretreatment and with ozone pre-treatment (10 s). XPS spectra of O 1s core level of HZO thin films deposited on TiN b) without pre-treatment and with ozone pre-treatment (10 s). STEM-EELS measurement results. EEL spectra for ozone pretreated and without pretreated samples at HZO/bottom TiN interface of c) N K edge and d) Ti L_{2,3} edge. e) O K-edges in the HZO film (see the inset image). Ozone pretreated and non-pretreated samples are indicated by red and black solid lines, respectively.

in TiO_2 peak intensity compared with the slight decrease in TiN and TiN_xO_y sub-oxide peak intensities is due to the effect of the thick TiO_2 layer generated by the intentional oxidation of TiN substrates by ozone treatment before HZO deposition. The TiO_2 layer formed in the above way can be expected to effectively suppress the oxygen scavenging effect of TiN from HZO. Therefore, we confirmed whether the intentional oxidation of the TiN surface through ozone pre-treatment could reduce the oxygen scavenging of TiN. As shown in Figure 2b the non-lattice oxygen in the HZO/TiN structure decreased from 22.3% to 16.2% after 10 s ozone pre-treatment. Although it is difficult to quantify oxygen vacancies with non-lattice oxygen extracted from the O 1s peak, the decrease in non-lattice oxygen indicates a decrease in oxygen vacancies.^[22]

Also, scanning transmission electron microscopy (STEM)-electron energy loss spectroscopy (EELS) measurement was performed to analyze the effect of ozone pre-treatment on the oxidation state at the interface in more detail. We measured the N K edge and Ti $L_{2,3}$ edge to confirm the oxidation effect that ozone pre-treatment has on the bottom TiN. We then measured the O K edge to show the electronic structure of the HZO thin film on TiN. Figure 2c shows the N K edge at the HZO/bottom TiN interface with and without ozone pre-treatment. For the non-treated interface, the pre-peak of N K is split by 2 eV (398 and 400 eV, arrow in Figure 2c), which is the typical characteristic of TiN.^[23] The split is derived from the transition from N 1s electrons to the empty state and a state formed by the hybridization between the N 2p and Ti 4b state. However, the peak split is broadened for the ozone pretreated interface (red line). This implies that the oxidation of the TiN surface induces TiN_xO_y sub-oxide formation. Subsequent reduction of the hybridization between N 2p and Ti 4b state led to a smeared N K edge. A comparison obtained from the Ti $L_{2,3}$

edges is shown in Figure 2d. The results revealed that the Ti $L_{2,3}$ doublets for the ozone pre-treated interface showed both peak splits and energy shifts to higher energy, proving the TiN surface is oxidized into TiO_2 . Formation of octahedral TiO_2 results in splitting the Ti 2p orbitals into two sub-levels of t_{2g} and e_g , and thus splitting of the $L_{2,3}$ doublets.^[24] It is also noticeable that the $L_{2,3}$ white lines shift to higher energies by ≈ 0.6 eV for the oxidized interface, indicating the transformation from TiN to TiO_2 phases.^[25] Therefore, TiN_xO_y sub-oxides and TiO_2 formed by ozone pre-treatment were confirmed via the EELS analysis as illustrated in the XPS measurements. We investigated the change of chemical bonding state of oxygen atoms at the HZO layer as displayed in Figure 2e, which shows the O K edges. Here, the intensity of the pre-edge (532.5 eV) for the ozone pre-treated HZO is prominent. On the other hand, the non-treated film showed a lower intensity. It has been reported that the crystalline HfO_2 presents sharp double peaks, 532.5 and 536 eV, due to the e_g-t_{2g} split.^[26–28] However, distorted coordination leads to peak broadening and reduces the pre-edge intensity at higher oxygen vacancy concentration.^[29] Therefore, a sharp double-peak of the ozone pre-treated HZO implies that the oxygen vacancy is reduced due to the formation of a diffusion blocking layer, TiN_xO_y sub-oxides, and TiO_2 at the HZO/bottom TiN interface. Moreover, we confirmed that the intensity of these sharp pre-edge peaks also appeared at the interface (see Figure S4, Supporting information). From the XPS analysis and EELS measurement results, proper oxidation of the TiN surface through ozone treatment both suppresses unwanted interfacial reactions using oxygen in the HZO thin film as an oxygen source and reduces oxygen vacancies to oxygen loss in the film.

The cause of the improvement of ferroelectric properties by ozone pre-treatment were further investigated by analyzing the structure and crystallinity of the thin films. Figure 3a,b shows

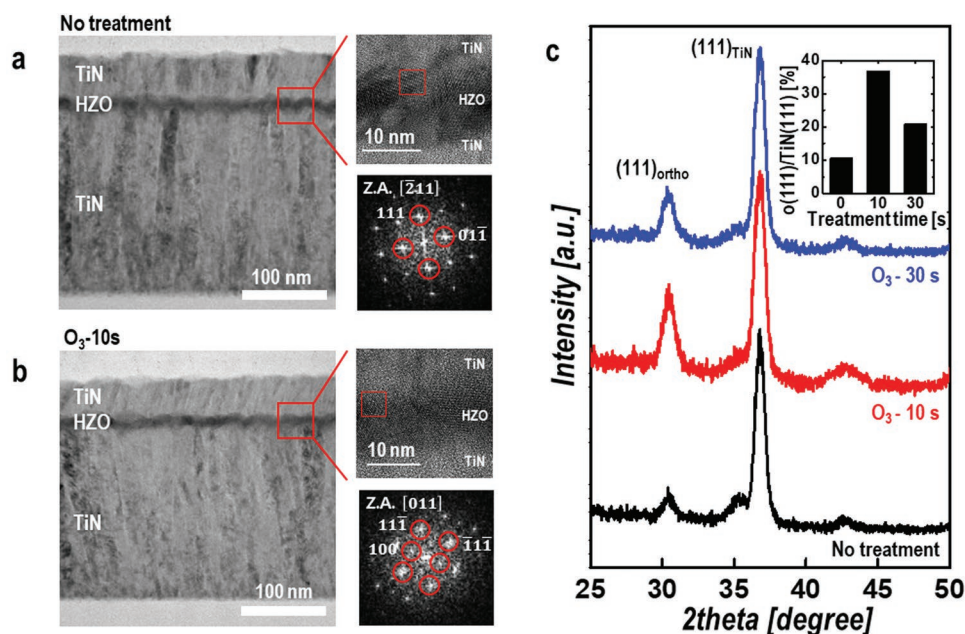


Figure 3. TEM bright-field images of MFM capacitors and corresponding oxygen EELS map. Wien filtered HRTEM results a) without pretreatment and b) ozone pretreatment samples. c) The GI-XRD spectra (linear scale) of HZO thin films on TiN substrate with and without ozone pretreatment. Inset: Intensity ratio of the orthorhombic (111) peak and TiN (111) peak.

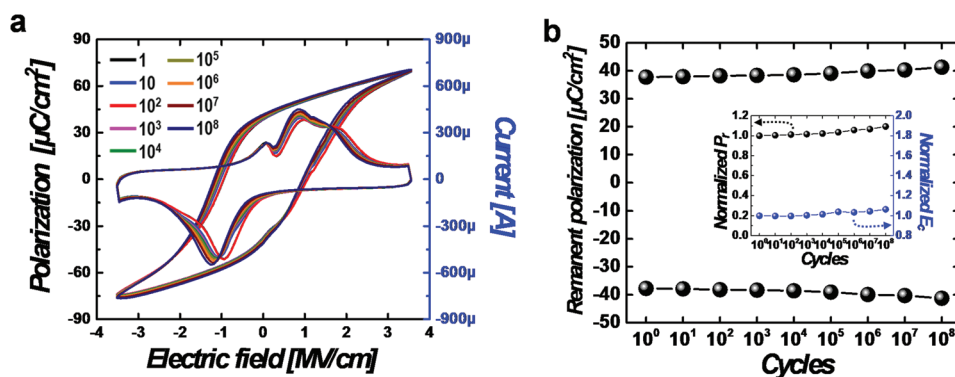


Figure 4. a) P - E and I - E loops of TiN/HZO/TiN capacitor with ozone pretreatment time of 10 s for the pristine state and the subsequently measured cycles. b) Variation of the positive remanent polarization and negative remanent polarization as a function of number of cycles measured at an applied electric field of 3.5 MV cm^{-1} . Inset: normalized curve of the remanent polarization and coercive field as a function of number of cycles.

transmission electron microscopy (TEM) bright-field images of MFM capacitors and the corresponding high-resolution TEM (HRTEM) image of the HZO thin film. The dark contrast layer of the HZO thin film ($\approx 10 \text{ nm}$) was grown on the columnar multi-grain TiN layer ($\approx 200 \text{ nm}$). Subsequently, a top TiN layer was deposited on the HZO film. So, TEM bright-field images showed that the HZO thin film is uniformly grown on the bottom TiN layer with and without ozone pre-treatment. In the HRTEM images, we observed the orthorhombic phase through fast Fourier transform (FFT) structure analysis in both samples, and this shows both samples can operate ferroelectrics. Figure 3c also shows the crystallinity of HZO thin films with and without ozone pre-treatment. GI-XRD spectra indicated that all HZO thin films were crystallized to the orthorhombic phase as with the FFT structure analysis of HRTEM. Interestingly, the orthorhombic (111) peak intensity (around $2\theta \approx 30.5^\circ$) of the ozone-treated samples increased remarkably compared to that of the untreated sample. In particular, the intensity ratio of the orthorhombic (111) and TiN (111) peak intensity increased more than three times in the case of the 10 s ozone-treated MFM sample, and it showed the maximum remanent polarization value. The ratio of orthorhombic (111) and TiN (111) peak intensities of MFM samples treated with 5 s O_2 plasma also increased by almost four times (see Figure S6, Supporting information). Zhou et al. reported the effects of oxygen vacancies in the HfO_2 bulk and interface (between TiN bottom electrode and HfO_2), on the non-centrosymmetric orthorhombic phase transformation by a DFT calculation. They claimed that the ferroelectric phase could be stable by reducing the energy difference between the ferroelectric and monoclinic phase in the following cases: 1. Oxygen vacancies are present in the bulk. 2. Absent or very small amounts are present at the interface.^[30] As seen in Figure 2 and Figure S4 (Supporting Information), this theoretical approach is in good agreement with the results of the present work. That is, the reduction of oxygen vacancies at the interface through TiN pre-treatment can improve the crystallinity of the orthorhombic phase, which causes an improvement in ferroelectricity. Therefore, we concluded that the improvement of ferroelectric properties through ozone pre-treatment was both due to the change in the interfacial properties and due to the increase in the crystallinity of the HZO thin film.

Finally, the switching endurance test for the sample with enhanced ferroelectric properties by ozone pre-treatment was examined. Figure 4a shows the P - E and I - E loops of HZO thin films deposited on the TiN bottom electrode after 10 s ozone treatment for the pristine state and subsequently measured cycles. The MFM capacitor exhibited almost identical P - E and I - E curves after up to 10^8 cycles. The normalized remanent polarization (P_r) and coercive field (E_c) values as a function of cycle number are shown in Figure 4b. For comparison, the endurance test result of the MFM capacitors as a function of ozone pre-treatment time are shown in Figure S7 (Supporting information). For the MFM capacitor without pre-treatment, a wake-up effect, a phenomenon in which the P_r value increases as the number of cycles increases, occurred at the beginning of the switching cycle. Failure due to hard breakdown was observed before 10^6 cycles, and measurement was possible only up to 10^5 cycles. However, the endurance characteristics were greatly improved as a result of applying ozone pre-treatment for 10 s before deposition of HZO thin films, as shown in Figure 4b. Even after 10^8 cycles at a relatively high electric field of 3.5 MV cm^{-1} , the values of P_r and E_c hardly changed, which means that the resistance to the wake-up effect and fatigue phenomena occurring in general HfO_2 -based ferroelectrics is excellent. After 10^8 cyclic measurements, the change in $2P_r$ value was very small, only $+7.03 \mu\text{C cm}^{-2}$ ($\approx 9.3\%$), which ensures the stable operation of ferroelectric-based devices formed using this process. Also, although there was an optimized interfacial oxidation condition in terms of remanent polarization, it was observed that sufficient interfacial oxidation could ensure improved endurance properties (see Figure S7, Supporting information). This improvement in endurance characteristics is thought to be due to the improvement of interface characteristics and reduction of oxygen vacancies through ozone pre-treatment. Generally, it is known that oxygen vacancy inside the ferroelectric thin film causes a wake-up effect and a fatigue effect as well. Oxygen vacancies inside the thin film are redistributed during the switching cycles, which causes a wake-up effect that changes the P_r value.^[31] Also, fatigue is caused by pinning of the domain wall due to bulk defects such as oxygen vacancies.^[17] Therefore, it was expected that a MFM capacitor with proper ozone pre-treatment would be able to reduce the formation of oxygen vacancies generated by unwanted interface

Table 1. Experimental reports on HfO₂-based ferroelectric capacitors in the literature.

Material	Method	Thick. [nm]	Electrodes Top/Bottom	Pr [$\mu\text{C cm}^{-2}$]	Ec [MV cm ⁻¹]	Endurance cycles/E-field [MV cm ⁻¹]	Reference
Y-doped HfO ₂	ALD	10	TiN/TiN	24	1.2	–	[33]
Gd-doped HfO ₂	ALD	27	TaN/TaN	35	<1.8	–	[34]
La-doped HfO ₂	ALD	10	TiN/TiN	23	<2	–	[35]
Hf _{0.5} Zr _{0.5} O ₂	ALD	5.1	TiN/TiN	4.1	–	10 ¹⁰ /4.7	[36]
Hf _{0.5} Zr _{0.5} O ₂	ALD	10	(Pt/TiN)/TiN	20.7	<2	10 ¹⁰ /3.5	[37]
Hf _{0.42} Zr _{0.58} O ₂	PA-AOD	13	TiN/Ge	30.6	1.8	10 ⁵ /2.3	[38]
(Hf,Zr)O ₂	ALD	5	Mo/TiN	40	2	10 ⁴ /4	[39]
(Hf,Zr)O ₂	ALD	5	TaN/TiN	25	1.5	10 ⁵ /4	[39]
La-doped (Hf,Zr)O ₂	ALD	10	TiN/TiN	15.5	1	10 ¹¹ /2.5	[40]
Hf _{0.5} Zr _{0.5} O ₂	ALD	10	W/W	32	<2	10 ⁴ /3	[41]
Hf _{0.25} Zr _{0.75} O ₂	PEALD	–	TiN/TiN	28.7	2.3	–	[42]
Hf _{0.5} Zr _{0.5} O ₂	ALD	10	TiN/TiN	24.5	1	–	[43]
(Hf,Zr)O ₂	ALD	10	TiN/TiN	36.5	2.01	10 ⁸ /3.5	This work

reactions between HZO thin films and the TiN bottom electrode during HZO deposition and post-annealing to form very stable HZO based MFM capacitors that were wake-up free with no significant degradation caused by fatigue.

To demonstrate the superiority of the proposed process in this study among the previously reported results, devices from the literature with relatively good P_r values and endurance properties are listed in **Table 1** and a more extensive list of data can be found in the paper reported by Park et al.^[32] Compared to previously reported results, the P_r value of the ferroelectric capacitor with ozone treatment proposed in this paper showed a very high value of $\approx 36.5 \mu\text{C cm}^{-2}$. Moreover, it was also confirmed that excellent endurance results without fatigue up to 10⁸ cycles even under a severe electric field of 3.5 MV cm⁻¹. Therefore, we concluded that intentional oxidation of the TiN bottom electrode through ozone pretreatment can be applied to various ferroelectric-based devices as a simple method of simultaneously improving remanent polarization and endurance characteristics.

3. Conclusion

We investigated the effect of an ozone pre-treatment process on the surface of the TiN bottom electrode (before HZO thin film deposition) on the physical and electrical properties of HZO thin films. As the ozone pre-treatment time increased, the remanent polarization value of the MFM capacitor increased and then decreased. The largest remanent polarization value ($2P_r = 73 \mu\text{C cm}^{-2}$) was observed for the optimized ozone pre-treatment process. Moreover, HZO thin films with optimized pre-treatment exhibited very stable ferroelectric properties without wake-up effects or significant fatigue up to 10⁸ cycles compared to samples without pre-treatment that showed hard breakdown at up to 10⁶ cycles. These results were interpreted in terms of the ability to suppress unwanted interfacial reactions in the thin film through intentional oxidation at the HZO/TiN

interface, as well as an increase in orthorhombic crystallinity, which is directly related to the improvement of ferroelectric properties. These results suggest a simple and novel strategy to effectively improve the performance and cycling endurance of devices in all applications using ferroelectric thin films in the form of MFM structures.

4. Experimental Section

Process details: The HZO ferroelectric thin films were formed on TiN (200 nm) bottom electrodes by ALD using a shower-head type reactor ((iOV d150, iSAC RESEARCH Co., Ltd.). The cocktail precursor consisting of cyclopentadienyl-tris(dimethylamino)-hafnium (Hf[Cp(NMe₂)₃], iChems Co., Ltd.) and cyclopentadienyl-tris(dimethylamino)-zirconium (Zr[Cp(NMe₂)₃], iChems Co., Ltd.) was used as a precursor for HZO deposition. The precursor canister with a bubbler-type was heated to a temperature of 85 °C. The precursor delivery lines, showerhead, and ALD reactor were maintained at 110 °C, 180 °C, and 320 °C, respectively. Ozone at 220 g m⁻³ and Ar gas (> 99.999% purity) were used as reactant and carrier gas, respectively. Before ferroelectric thin film deposition, pre-treatment using ozone was conducted for intended oxidation of the TiN surface to investigate the effect of surface oxidation of TiN on the electrical properties of TiN/HZO/TiN ferroelectric capacitors. Then, the ALD processes for HZO deposition were carried out without a vacuum break under self-limiting growth conditions (10 s of cocktail precursor injection – 15 s of precursor purge – 6 s of ozone pulse – 15 s of final purge). The growth per cycle at saturation conditions was $\approx 0.88 \text{ \AA cycle}^{-1}$, and the deposited thickness of HZO thin films on Si substrates increased very slightly with increasing ozone pre-treatment time but was almost same (see Figure S1, Supporting information). For the formation of the top electrodes, the TiN (100 nm) dots were deposited via sputtering using a shadow mask with a diameter of 200 μm . After a top electrode deposition, post-metallization annealing was performed at 500 °C for 10 s in a N₂-atmosphere using a rapid thermal annealing process for HZO crystallization. The details of the process flow of fabricating MFM capacitors are shown in Figure 1a.

Thin Films Characterization: The deposited thickness of HZO thin films was measured using spectroscopic ellipsometry (SE MG-1000, Nano View). The crystal structure of the HZO thin films was characterized via grazing-angle incidence X-ray diffraction (GI-XRD, SmartLab, Rigaku) using Cu-K α radiation ($\lambda = 1.5405 \text{ \AA}$) with an incidence angle of 1° at the

Korea Basic Science Institute (Daegu). The chemical binding state of the interface of HZO thin films and TiN substrates was scrutinized using 4 nm-thick HZO thin films deposited on TiN via X-ray photoemission spectroscopy (XPS, K-alpha plus, Thermo Scientific) analysis. The capacitance–voltage (C–V) and current–voltage (I–V) measurements were carried out using a semiconductor characterization system (4200-SCS, Keithley) at room temperature. Polarization–electric field (P–E) measurements and switching endurance tests were also performed at room temperature using a semiconductor characterization system (Keithley, 4200-SCS) with a 4225-PMU module.

Electron Microscopy Characterization: Cross-sectional samples of ozone pretreated and non-pretreated MFM capacitors were prepared using a FIB FEI Quanta 3D FEG apparatus for TEM and STEM analysis. Microscopic data were acquired using a monochromated Cs-corrected TEM (Mono ARM200, JEOL) operated at 200 kV. High-resolution TEM (HRTEM) and corresponding FFT analysis for orthorhombic HZO crystals was performed using the electron diffraction simulation software (Single Crystal v4.14, Crystal Maker Software Ltd.). Corresponding crystal information files of the crystal structures were collected from the Materials Project database (<https://www.materialsproject.org/>). The Materials Project ID of orthorhombic HfO₂ is 685 097. The space group of the orthorhombic HfO₂ (#685 097) is Pca2₁ with cell parameters of $a = 5.040 \text{ \AA}$, $b = 5.074 \text{ \AA}$, $c = 5.269 \text{ \AA}$ and $\alpha = \beta = \gamma = 90^\circ$. HRTEM images were Wien filtered to remove contributions from amorphous phases. The EELS spectra were collected at sub-nanometer resolution with the Gatan Continuum HR 1066 spectrometer. The energy resolution of EELS was set to 0.55 eV using a monochromator. The energy dispersion of 0.3 eV channel⁻¹ was chosen to get the N K, Ti L_{2,3}, and O K energy loss near edge spectra (ELNES). The acquisition of the spectrum was performed at a dwell time of 0.5 s pixel⁻¹. Background was subtracted, and the plural scattering contributions were removed using the Fourier-ratio deconvolution technique.

Supporting Information

Supporting Information is available from the Wiley Online Library or from the author.

Acknowledgements

H.-B.K. and K.S.D. contributed equally to this work. This research was supported by a National Research Foundation of Korea (NRF) grant funded by the Korean government (MSIP) (No. 2019R1C1C1002982, 2020M3F3A2A01081240).

Conflict of Interest

The authors declare no conflict of interest.

Data Availability Statement

The data that support the findings of this study are available from the corresponding author upon reasonable request.

Keywords

atomic layer deposition, endurance test, ferroelectric capacitors, Hf_xZr_{1-x}O₂ thin films, interface treatment

Received: December 22, 2021

Revised: March 17, 2022

Published online: April 7, 2022

- [1] T. Böscke, J. Müller, D. Bräuhaus, U. Schröder, U. Böttger, *Appl. Phys. Lett.* **2011**, *99*, 102903.
- [2] M. H. Park, Y. H. Lee, H. J. Kim, Y. J. Kim, T. Moon, K. D. Kim, J. Mueller, A. Kersch, U. Schroeder, T. Mikolajick, *Adv. Mater.* **2015**, *27*, 1811.
- [3] S. Mueller, J. Müller, R. Hoffmann, E. Yurchuk, T. Schlösser, R. Boschke, J. Paul, M. Goldbach, T. Herrmann, A. Zaka, *IEEE Trans. Electron Devices* **2013**, *60*, 4199.
- [4] K. Florent, M. Pesic, A. Subirats, K. Banerjee, S. Lavizzari, A. Arreghini, L. Di Piazza, G. Potoms, F. Sebaai, S. McMitchell, presented at 2018 IEEE Int Electron Devices Meeting (IEDM) **2018**.
- [5] B. Zeng, M. Liao, Q. Peng, W. Xiao, J. Liao, S. Zheng, Y. Zhou, *IEEE J. Electron Devices Soc.* **2019**, *7*, 551.
- [6] S. Oh, T. Kim, M. Kwak, J. Song, J. Woo, S. Jeon, I. K. Yoo, H. Hwang, *IEEE Electron Device Lett.* **2017**, *38*, 732.
- [7] T. Ali, P. Polakowski, S. Riedel, T. Büttner, T. Kämpfe, M. Rudolph, B. Pätzold, K. Seidel, D. Löhr, R. Hoffmann, *Appl. Phys. Lett.* **2018**, *112*, 222903.
- [8] J. P. Silva, K. C. Sekhar, H. Pan, J. L. MacManus-Driscoll, M. Pereira, *ACS Energy Lett.* **2021**, *6*, 2208.
- [9] S. Dutta, P. Buragohain, S. Glinsek, C. Richter, H. Aramberri, H. Lu, U. Schroeder, E. Defay, A. Gruverman, J. Íñiguez, *Nat. Commun.* **2021**, *12*, 7301.
- [10] D. Zhou, J. Xu, Q. Li, Y. Guan, F. Cao, X. Dong, J. Müller, T. Schenk, U. Schröder, *Appl. Phys. Lett.* **2013**, *103*, 192904.
- [11] P. D. Lomenzo, Q. Takmeel, C. Zhou, C. M. Fancher, E. Lambers, N. G. Rudawski, J. L. Jones, S. Moghaddam, T. Nishida, *J. Appl. Phys.* **2015**, *117*, 134105.
- [12] H. J. Kim, M. H. Park, Y. J. Kim, Y. H. Lee, T. Moon, K. Do Kim, S. D. Hyun, C. S. Hwang, *Nanoscale* **2016**, *8*, 1383.
- [13] R. Cao, B. Song, D. Shang, Y. Yang, Q. Luo, S. Wu, Y. Li, Y. Wang, H. Lv, Q. Liu, *IEEE Electron Device Lett.* **2019**, *40*, 1744.
- [14] K.-Y. Chen, P.-H. Chen, R.-W. Kao, Y.-X. Lin, Y.-H. Wu, *IEEE Electron Device Lett.* **2017**, *39*, 87.
- [15] S. Starschich, S. Menzel, U. Böttger, *Appl. Phys. Lett.* **2016**, *108*, 032903.
- [16] D.-P. Xu, L.-J. Yu, X.-D. Chen, L. Chen, Q.-Q. Sun, H. Zhu, H.-L. Lu, P. Zhou, S.-J. Ding, D. W. Zhang, *Nanoscale Res. Lett.* **2017**, *12*, 311.
- [17] E. D. Grimley, T. Schenk, X. Sang, M. Pešić, U. Schroeder, T. Mikolajick, J. M. LeBeau, *Adv. Electron. Mater.* **2016**, *2*, 1600173.
- [18] A. Pal, V. K. Narasimhan, S. Weeks, K. Littau, D. Pramanik, T. Chiang, *Appl. Phys. Lett.* **2017**, *110*, 022903.
- [19] T. Mittmann, M. Materano, P. D. Lomenzo, M. H. Park, I. Stolichnov, M. Cavalieri, C. Zhou, C. C. Chung, J. L. Jones, T. Szyjka, *Adv. Mater. Interfaces* **2019**, *6*, 1900042.
- [20] Y. Li, R. Liang, B. Xiong, H. Liu, R. Zhao, J. Li, T. Liu, Y. Pang, H. Tian, Y. Yang, *Appl. Phys. Lett.* **2019**, *114*, 052902.
- [21] C. Ernsberger, J. Nickerson, A. Miller, J. Moulder, *J. Vac. Sci. Technol. A* **1985**, *3*, 2415.
- [22] H. I. Jaim, S. Lee, X. Zhang, I. Takeuchi, *Appl. Phys. Lett.* **2017**, *111*, 172102.
- [23] P. Longo, H. Zhang, R. Twisten, *Mater. Sci. Semicond. Process.* **2017**, *65*, 44.
- [24] D. W. Fischer, *J. Appl. Phys.* **1970**, *41*, 3561.
- [25] I. Abdallah, C. Dupressoire, L. Laffont, D. Monceau, A. V. Put, *Corros. Sci.* **2019**, *153*, 191.
- [26] D. W. McComb, *Phys. Rev. B* **1996**, *54*, 7094.
- [27] G. Wilk, D. Muller, *Appl. Phys. Lett.* **2003**, *83*, 3984.
- [28] T. Mizoguchi, M. Saitoh, Y. Ikuhara, *J. Phys. Condens. Matter.* **2009**, *21*, 104212.
- [29] J. H. Jang, H.-S. Jung, J. H. Kim, S. Y. Lee, C. S. Hwang, M. Kim, *J. Appl. Phys.* **2011**, *109*, 023718.
- [30] Y. Zhou, Y. Zhang, Q. Yang, J. Jiang, P. Fan, M. Liao, Y. Zhou, *Comput. Mater. Sci.* **2019**, *167*, 143.

- [31] M. Park, H. Kim, Y. Kim, T. Moon, K. Kim, Y. Lee, S. Hyun, C. Hwang, *J. Mater. Chem. C* **2015**, *3*, 6291.
- [32] M. H. Park, D. H. Lee, K. Yang, J.-Y. Park, G. T. Yu, H. W. Park, M. Materano, T. Mittmann, P. D. Lomenzo, T. Mikolajick, *J. Mater. Chem. C* **2020**, *8*, 10526.
- [33] J. Müller, U. Schröder, T. Böschke, I. Müller, U. Böttger, L. Wilde, J. Sundqvist, M. Lemberger, P. Kücher, T. Mikolajick, *J. Appl. Phys.* **2011**, *110*, 114113.
- [34] M. Hoffmann, U. Schroeder, T. Schenk, T. Shimizu, H. Funakubo, O. Sakata, D. Pohl, M. Drescher, C. Adelman, R. Materlik, *J. Appl. Phys.* **2015**, *118*, 072006.
- [35] C. Mart, K. Kühnel, T. Kämpfe, S. Zybelle, W. Weinreich, *Appl. Phys. Lett.* **2019**, *114*, 102903.
- [36] G. Walters, A. Shekhawat, N. G. Rudawski, S. Moghaddam, T. Nishida, *Appl. Phys. Lett.* **2018**, *112*, 192901.
- [37] T. Kim, J. Park, B.-H. Cheong, S. Jeon, *Appl. Phys. Lett.* **2018**, *112*, 092906.
- [38] C. Zacharaki, P. Tsipas, S. Chaitoglou, S. Fragkos, M. Axiotis, A. Lagoyiannis, R. Negrea, L. Pintilie, A. Dimoulas, *Appl. Phys. Lett.* **2019**, *114*, 112901.
- [39] K.-T. Chen, C.-Y. Liao, C. Lo, H.-Y. Chen, G.-Y. Siang, S. Liu, S.-C. Chang, M.-H. Liao, S.-T. Chang, M. Lee, presented at 2019 Electron Devices Technology and Manufacturing Conference (EDTM) **2019**.
- [40] M. G. Kozodaev, A. G. Chernikova, E. V. Korostylev, M. H. Park, R. R. Khakimov, C. S. Hwang, A. M. Markeev, *J. Appl. Phys.* **2019**, *125*, 034101.
- [41] A. Kashir, H. Kim, S. Oh, H. Hwang, *ACS Appl. Electron. Mater.* **2021**, *3*, 629.
- [42] D. Das, V. Gaddam, S. Jeon, *IEEE Electron Device Lett.* **2019**, *41*, 34.
- [43] S. J. Kim, J. Mohan, J. Lee, J. S. Lee, A. T. Lucero, C. D. Young, L. Colombo, S. R. Summerfelt, T. San, J. Kim, *Appl. Phys. Lett.* **2018**, *112*, 172902.